Effects of Lung Surfactant Proteins, SP-B and SP-C, and Palmitic Acid on Monolayer Stability

Junqi Ding,* Dawn Y. Takamoto,* Anja von Nahmen,* Michael M. Lipp,* Ka Yee C. Lee,† Alan J. Waring,‡ and Joseph A. Zasadzinski*

*Department of Chemical Engineering, University of California, Santa Barbara, California 93106; †Department of Chemistry, University of Chicago, Chicago, Illinois 60637; and ‡Department of Pediatrics, University of California, Los Angeles, California 90059 USA

ABSTRACT Langmuir isotherms and fluorescence and atomic force microscopy images of synthetic model lung surfactants were used to determine the influence of palmitic acid and synthetic peptides based on the surfactant-specific proteins SP-B and SP-C on the morphology and function of surfactant monolayers. Lung surfactant-specific protein SP-C and peptides based on SP-C eliminate the loss to the subphase of unsaturated lipids necessary for good adsorption and respreading by inducing a transition between monolayers and multilayers within the fluid phase domains of the monolayer. The morphology and thickness of the multilayer phase depends on the lipid composition of the monolayer and the concentration of SP-C or SP-C peptide. Lung surfactant protein SP-B and peptides based on SP-B induce a reversible folding transition at monolayer collapse that allows all components of surfactant to be retained at the interface during respreading. Supplementing Survanta, a clinically used replacement lung surfactant, with a peptide based on the first 25 amino acids of SP-B also induces a similar folding transition at monolayer collapse. Palmitic acid makes the monolayer rigid at low surface tension and fluid at high surface tension and modifies SP-C function. Identifying the function of lung surfactant proteins and lipids is essential to the rational design of replacement surfactants for treatment of respiratory distress syndrome.

INTRODUCTION

Treating premature infants with respiratory distress syndrome with replacement surfactants derived from natural and synthetic sources has significantly reduced neonatal mortality (Robertson and Halliday, 1998). Native surfactant is complex, and includes multiple lipid species and four specific proteins (SP-A, -B, -C, and -D). In fact, the lipid and protein composition of native surfactant is quite different even between cows and pigs, the sources of most animal-based replacement surfactants (Bernhard et al., 2000). The composition variations among different clinically used replacement surfactants are even greater and depend both on the nature of extraction from the animal sources and the choice of "additives" (Bernhard et al., 2000). However, a fairly limited number of components are generally agreed to be essential to surfactant performance in vivo and simplify the choices for model systems for study (Robertson and Halliday, 1998; Goerke, 1998). These include saturated dipalmitoylphosphatidylcholine (DPPC), unsaturated phosphatidylcholines and phosphatidylglycerols (PG) (Veldhuizen et al., 1998), and the two amphiphilic surfactant-specific proteins, SP-B (Hawgood et al., 1998) and SP-C (Johansson, 1998). Palmitic acid (PA), while found at low concentrations in native surfactants (Veldhuizen et al., 1998), is a common additive to replacements surfactants such as Survanta (Bernhard et al., 2000). However, the function of PA in the monolayer in native or replacement surfactants is not well understood.

Proper pulmonary function requires low surface tensions during expiration to minimize the work of breathing (Schürch et al., 1976). This would seem to require that lung surfactant form rigid monolayers capable of low surface tension on compression. However, lung surfactant monolayers also must be fluid enough to spread rapidly during the expansion of the interface that accompanies inspiration (Bastacky et al., 1995). Although the individual components of lung surfactant are either good at lowering surface tension (DPPC, especially when mixed with PA) or fluidizing the monolayer (unsaturated PG and PC, proteins), *no* single lipid or protein exhibits both properties.

DPPC forms a semi-crystalline monolayer capable of surface tensions near zero when fully compressed. However, DPPC fails as a lung surfactant (Poulain and Clements, 1995; Robertson and Halliday, 1998) as it is slow to adsorb from aqueous suspension and respreads slowly when compression is relieved. This help explains the significant fraction of unsaturated phospholipids and hydrophobic proteins in native surfactant (Veldhuizen et al., 1998; Hawgood et al., 1998; Johansson, 1998). Although unsaturated lipids and proteins facilitate surfactant adsorption and spreading, they collapse at relatively high surface tensions via the ejection of material from the monolayer (Tchoreloff et al., 1991; Lipp, 1997; Lipp et al., 1998; Schürch et al., 1976; Nag et al., 1998). The ejected material does not readily reincorporate into the monolayer on expansion (Lipp et al., 1998) (see Fig. 2).

The contradictory requirements of lung surfactant monolayers have led to the "squeeze-out" theory of lung surfactant function: the unsaturated lipids and proteins in lung

Received for publication 10 March 2000 and in final form 12 February 2001.

Address reprint requests to Joseph A. Zasadzinski, Department of Chemical Engineering, University of California, Santa Barbara, Santa Barbara, CA 93106-5080. Tel.: 805-893-4769; Fax: 805-893-4731; E-mail: gorilla@engineering.ucsb.edu.

0006-3495/01/05/2262/11 $2.00

surfactant are selectively removed or "squeezed-out" from the monolayer during compression, leading to a DPPC-enriched monolayer capable of low surface tension. However, in vitro studies of captive (Schürch et al., 1998; Ingenito et al., 1999) and pulsating (Krueger and Gaver, 1999) air bubbles in contact with aqueous surfactant show that the necessary mass transfer to the interface requires that the surfactant remain within a few nanometers of the interface. Hence, current thought is that the lipids and proteins "squeezed-out" from the monolayer occupy a "surface associated reservoir" near the interface (Schürch et al., 1998). In vivo, electron microscopy has shown areas within alveoli that have discontinuous multilayer patches along with continuous monolayers (Bastacky et al., 1995; Schürch et al., 1998; Tchoreloff et al., 1991).

Langmuir monolayers at the air-water interface provide experimentally useful model systems for studies of lung surfactants and other amphiphilic molecules. Care is necessary to extrapolate Langmuir monolayer behavior to lung surfactant behavior in vivo, but general correlations between in vitro and in vivo behavior are starting to emerge (Bernhard et al., 2000; Cochrane and Revak, 1991; Goerke, 1998; Jobe, 1998; Lipp et al., 1996, 1998). The phase behavior of surfactants in two dimensions is determined by pressure-area isotherms. Additional information about the morphology of the monolayer domains is accessible by modern visualization techniques such as fluorescence and atomic force microscopy. We present isotherms, fluorescence microscopy, and atomic force microscopy to show that the lung surfactant-specific proteins SP-B and SP-C and peptides based on these proteins interact with the various lipid species to create localized monolayer-to-multilayer transitions that provide low surface tensions on compression and rapid and repeatable respreading on expansion. These lipid- and protein-induced transitions are modified by changes in the monolayer mechanical properties induced by the addition of palmitic acid to DPPC/POPG (palmitoyloleoylphosphatidylglycerol) monolayers. The net result of these interactions is that all of the lipid and protein components of lung surfactant remain at the interface (or at least within Schürch's "surface associated reservoir" (Schürch et al., 1998)) during the entire compression and expansion cycle; removal of a significant fraction of the unsaturated and protein components of the monolayer, that is, classical "squeeze-out," is not required for low surface tensions. Identifying the roles of the individual lipid and protein species in lung surfactants is essential to more rational design of replacement lung surfactants for treatment of respiratory distress syndrome.

MATERIALS AND METHODS

Protein synthesis

Surfactant protein B is a 78-residue, lipid-associating protein found in mammalian lung surfactant (Hawgood et al., 1998). Each monomer has disulfide links at the mid-sequence, N-terminal, and C-terminal sections, suggesting the main chain may assume a hairpin-like format. The native SP-B protein has a net positive charge of 8 (10 cationic and 2 anionic residues), a large fraction of strongly hydrophobic residues, and has four amphipathic helical segments with the helical axes oriented parallel to the interface (Gordon et al., 1996, 2000). Preparations from native material are generally homodimeric.

The full-length human 78-amino acid sequence of surfactant protein ($SP\text{-}B_{1–78}$) is shown below. In each sequence, the charged residues are indicated with a "+" or a "−" sign:

```
    1          +   ++       +25
NH2-FPIPLPYCWLCRALIKRIQAMIPKG
   +       +                50
 ALRVAVAQVCRVVPLVAGGICQCLA
 −+      −   +        +   + 78
  ERYSVILLDTLLGRMLPQLVCRLVLRCS-COOH
```

(Full-length SP-B)

To simplify synthesis and to try to isolate the essential features of SP-B, a peptide based on the N-terminus of SP-B known as $SP\text{-}B_{1–25}$ was synthesized (Bruni et al., 1991). $SP\text{-}B_{1–25}$ is able to recreate many of the functions of the full-length SP-B protein both in vivo and in vitro (Lipp et al., 1996, 1998; Longo et al., 1993). Both full-length SP-B and $SP\text{-}B_{1–25}$ form amphipathic α-helices (Gordon et al., 1996, 2000) that help orient the protein at the interface. The amino acid sequence of $SP\text{-}B_{1–25}$ is as follows:

```
     1          +   ++      +25
  NH2-FPIPLPYCWLCRALIKRIQAMIPKG-COOH
```

($SP\text{-}B_{1–25}$)

SP-C is a 4.2-kDa, dipalmitoylated, 35-residue peptide, of which 23 residues are hydrophobic. SP-C has a transbilayer orientation similar to that of integral membrane proteins and adopts an α-helical conformation between residues 9 and 34 (Johansson, 1998):

```
        +   **     ++
   NH2-LRIPCCPVNLKRLLVVVVV
    VVLVVVVIVGALLMGL-COOH
```

(SP-C)

The N-terminal segment includes two palmitoylcysteinyls (**) and is flexibly disordered in solution. The length of the α-helix is ~3.7 nm and orients along the acyl chains of lipids in a monolayer or bilayer environment (Gericke et al., 1997; Johansson, 1998). The hydrophobic character of SP-C and palmitoylation makes native SP-C very difficult to synthesize. We synthesized an analog of SP-C, SP-C*ff* (based on work by Byk-Gulden Pharmaceutical, Konstance, Germany) (Ikegami et al., 1998; Ikegami and Jobe, 1998) in which the palmitoylated cysteines are replaced by phenylalanine residues (**):

```
        +   **     ++
   NH2-LRIPFFPVNLKRLLVVVVV
    VVLVVVVIVGALLMGL-COOH
```

(SP-Cff)

This mutant protein performs nearly identically to the native SP-C in animal models (Davis et al., 1998; Ikegami et al., 1998; Ikegami and Jobe, 1998) and is significantly easier to synthesize. This mutant is similar to dog SP-C, which has only a single palmitoylated cysteine, with the second replaced by phenylalanine (Batenburg and Haagsman, 1998).

Peptide synthesis reagents including Fmoc amino acids and coupling solvents were obtained from Applied Biosystems (Foster City, CA). All organic solvents used for sample synthesis, purification and preparation were HPLC grade or better from Aldrich Chemical Co. (Milwaukee, WI).

The full-length and peptide versions of SP-B were synthesized by the solid-phase method of Merrifield, with the use of a *tert*-butyloxycarbonyl strategy or by Fmoc strategies (UCLA Peptide Synthesis Facility). The crude peptides were purified by C4-column (Vydac, Hesperia, CA) reversed-phase high-performance liquid chromatography (HPLC) with a mixture of water, acetonitrile, and 0.1% trifluoroacetic acid. Solvents from HPLC and ion-pairing agents were removed from the purified peptides by vacuum centrifugation, and the expected molecular mass of the peptide was obtained by fast atom bombardment mass spectrometry or electrospray mass spectroscopy (UCLA Center for Molecular and Medical Sciences Mass Spectrometry). Quantitative amino acid composition for the peptide was determined at the UCLA Protein Microsequencing Facility.

SP-C*ff* was synthesized on a 0.25 mmol scale using an Applied Biosystems 431A peptide synthesizer using FastMoc chemistry. The peptide was synthesized using a prederivatized Fmoc-leu-PEG-PS resin (PerSeptive Biosystems, Farmington, MA) having a substitution of 0.18 mmol/g. Residues Gly-33 to Gly-29 were single-coupled, while the remaining sequence was double-coupled to the N-terminus. Cleavage and deprotection of the peptide-resin was carried out in a 10-ml TFA, 0.25-ml ethanedithiol, 0.5-ml thioanisole, and 0.5-ml water mixture for 1.5 h. The reaction mixture was then removed by vacuum filtration through a medium porosity fritted glass funnel and the resin washed sequentially with 1 ml TFA, then 5 ml DCM, and finally with 5 ml of isopropanol/TFA (95:5, v/v) to ensure separation of the peptide from the resin.

The crude peptide was purified by reverse-phase HPLC with a Vydac C4 column (1 cm × 20 cm; The Separations Group, Hesperia, CA) using a water-acetonitrile/isopropanol (1:1, v/v) linear gradient with 0.1% TFA as an ion-pairing agent. The molecular weight of the full length SP-C*ff* was confirmed by MALDI-TOF mass spectrometry using a Voyager RP-RBT2 reflection time of flight mass spectrometer (PerSeptive Biosystems, Inc., Framingham, MA). α-Cyano-4-hydroxycinnamic acid was used as a matrix and bovine insulin was used as an internal calibration standard.

Preparation of model monolayers

Model monolayers were spread from organic solvents by mixing the proteins or peptides with the appropriate amounts of saturated DPPC, unsaturated POPG, and PA (all from Avanti Polar Lipids, Inc., Alabaster, AL; 99% purity) in the weight ratios of 68:22:8 in 3:1 chloroform/methanol (Fisher Spectranalyzed). This lipid mixture is a close functional mimic to natural lung surfactants both in vitro and in vivo (Tanaka et al., 1986). However, the composition of native surfactant varies significantly from species to species, and the compositions of replacement surfactants vary even more due to difficulties in extraction and in the number and type of additives used, so there is no universally accepted surfactant composition as yet (Bernhard et al., 2000; Mizuno et al., 1995). The fluorescent probe 1-palmitoyl, 6-(*N*-7-nitrobenz-2-oxa-1,3-diazol-4-yl-)-PG (NBD-PG, Molecular Probes, Eugene, OR) was added at lipid mole ratios of 0.5 to 1%. The fluorescent probe segregates to disordered or fluid phases, which then appear bright in images; the probe is absent from the solid or liquid condensed phases, which appear black or dark (Knobler and Desai, 1992).

Survanta was purchased from Ross Laboratories (Columbus, OH). Survanta is natural bovine lung extract containing phospholipids, neutral lipids, fatty acids, and the surfactant-associated proteins SP-B and SP-C, to which DPPC, PA, and tripalmitin are added to standardize the composition. The approximate composition is 25 mg/ml phospholipid (of which ~50–60% is DPPC), 0.5–1.75 mg/ml triglycerides, 1.5–3.5 mg/ml free fatty acids. Survanta contains both native SP-B and SP-C, but in concentrations less than that of native surfactant due to losses during the extraction process. For these experiments, the lipids and proteins were diluted in 0.9% sodium chloride solution at a total concentration of ~2 mg/ml. For fluorescence experiments, NBD-PG was added to the Survanta by suspending the dye in the same sodium chloride solution, then adding a small percentage (0.5 wt %) to the Survanta solution by gentle swirling. Additional SP-B peptide was added by the same procedure. The Survanta suspension was spread at the interface by depositing small drops of the aqueous suspension onto the subphase surface.

All other monolayers were spread from a 3:1 chloroform/methanol spreading solution at typical concentrations of 0.5–1 mg/ml onto a 150 mM NaCl, 5 mM CaCl, 0.2 mM $NaHCO_3$, pH 6.9 subphase in a temperature-controlled microfluorescence film balance (Lipp et al., 1997a; Lipp, 1997). The trough is milled from a solid piece of Teflon with a working surface area of ~120 cm^2 and a subphase volume of ~150 ml. A single Teflon barrier runs linearly along the top edge of the trough and is driven by a motorized translation stage. The barrier is spring-loaded against the trough and the ends of the barrier in contact with the well edges are beveled at an angle of ~10° to minimize leakage of surfactant. Temperature control of the subphase is achieved through the use of nine thermoelectric cooling elements. The trough can be operated over a temperature range of 10–50°C. A simple feedback loop allows for measurement and control of the subphase temperature. The surface pressure is measured by a Wilhelmy plate-type transducer with a filter-paper plate (R&K, Wiesbaden, Germany).

For fluorescence imaging, a Nikon Optiphot with the stage removed is positioned above the trough. A 40× power long-working-distance objective designed for use with fluorescence systems is used. The trough is mounted on a motorized *xyz* translation stage: the *z* axis is used for focusing and the *x* and *y* axes are used to scan over different regions. A 100-watt high-pressure mercury lamp was used for excitation. A dichroic mirror/barrier filter assembly is used to direct the excitation light onto the monolayer (with a normal angle of incidence) and to filter the emitted fluorescence. The emitted fluorescence is collected by the objective and detected via a Silicon Intensified Target (SIT) camera. Images are recorded by a JVC super VHS VCR and digitized via a Scion frame grabber. The resulting digitized images are processed and analyzed following a custom-designed protocol (Lipp et al., 1997b).

The monolayers were examined over a range of temperatures between 30 and 37°C; for these lipid and protein mixtures there was no significant difference in isotherms or morphology over this temperature range (Lipp et al., 1997a; Takamoto, 1999). Due to the increased convection and leakage around the barriers at the higher temperature, transfers for AFM were done primarily at 30°C (Lee et al., 1998). All isotherms presented are typical; each isotherm was repeated numerous times to ensure reproducibility. Compressions were done quasi-statically: the typical time for a compression-expansion cycle was ~1 h. No variations of the isotherms were found for rates twice as fast or as slow.

Selected monolayers were transferred to mica substrates for AFM using a custom-built monolayer transfer system (Lee et al., 1998). A modified Nanoscope III FM (Digital Instruments, Santa Barbara, CA) was used for imaging. A low-resolution fluorescence optical microscope was used to position the AFM tip onto specific regions of the sample (Lee et al., 1998). Once the desired regions were located, AFM imaging was done with a 150 μm × 150 μm (J) scanner in contact mode. Silicon nitride tips with a spring constant of 0.12 N/m were used. Exerting large forces on the sample was a concern during imaging, so samples were checked often for deformation. This was done by imaging for a few minutes on a smaller region (~20 μm), then zooming out to check whether damage had been done to the scanned region.

Monolayer mechanical properties were measured using a custom-built monolayer viscometer based on a design by Brooks et al. (1999). A dual-barrier custom-built trough was equipped with parallel hydrophilic glass plates spaced 1.5 cm apart to create a 10-cm-long flow cell within the trough. A small magnetic needle (~1 cm long and 0.5 mm in diameter) in a Teflon boat was floated on the air-water interface between the two glass plates. A force was applied parallel to the long axis of the needle by a magnetic field gradient created by a pair of Helmholtz coils located on opposite sides of the trough. The magnitude of the magnetic field gradient, and hence the force on the needle, is proportional to the current in the coils. The needle position is followed with a video camera to determine the velocity of the needle. The needle rapidly comes to a steady velocity for a given force. The velocity is proportional to the viscosity of the monolayer; high needle velocities imply low monolayer viscosity, low needle veloci-

ties imply a higher monolayer viscosity. As the monolayer is certainly non-Newtonian, we cannot report a single viscosity, but rather just compare the terminal velocities at a given applied force. The velocity is normalized with respect to the needle velocity of the clean subphase. Temperature control was not available for this trough, so all measurements were done at ~25°C. The needle sinks at sufficiently high surface pressure, so measurements are limited to <50 mN/m.

RESULTS

Fig. 1 *A* shows typical cyclic isotherms (compression-expansion-compression) for the DPPC/POPG/PA, 68:22:8 (wt/wt/wt) model lipid mixture on a buffered saline subphase (150 mM NaCl, 5 mM CaCl, 0.2 mM NaHCO3, pH = 6.9) at 30°C without protein. The surface pressure, π, is the difference between the bare water surface tension (~72 mN/m for saline at 30°C) and the measured surface tension, γ: $\pi = 72 - \gamma$. Hence, a high surface pressure corresponds to a low surface tension. While the lipid mixture achieves high surface pressures, the second compression is shifted to lower area per molecule due to the selective removal, or squeeze-out of the unsaturated POPG (Lipp, 1997; Takamoto, 1999). By the second compression, most of the POPG has been lost to the subphase irreversibly. The collapse pressure of a monolayer is the highest surface pressure or lowest surface tension attainable before the film fails. High and reproducible collapse pressures are essential to minimizing the work of breathing. However, for the lipids alone, on repeated compression, the collapse pressure steadily decreased.

Fig. 1 *B* shows the change in the isotherm on addition of 2 wt % SP-C*ff* peptide (Davis et al., 1998) to the DPPC/POPG/PA, 68:22:8 (wt/wt/wt) lipid mixture at 30°C. For the second and subsequent compressions, the peptide induces a break in the isotherm at a surface pressure of ~50 mN/m and the offset in molecular area is reduced, especially at high surface pressure. The protein helps retain the unsaturated lipid components in the surface film. The maximum surface pressure increases to ~70 mN/m on the second and subsequent compressions. For these lipid and protein mixtures there was no significant difference in isotherms or morphology over the temperature range of 30–37°C. (Lipp et al., 1997a; Takamoto, 1999).

Contact mode AFM images of the SP-C*ff* containing monolayers show the change in morphology at surface pressures above and below the break in the isotherm. Fig. 2 *A* shows coexisting solid (*light gray*) and fluid (*dark gray*) phase domains in a DPPC/POPG/PA/SP-C*ff*, 68:22:8:2 (wt/wt/wt/wt) monolayer transferred at a surface pressure of 45 mN/m at 30°C (Lee et al., 1998). The domain sizes and shapes are consistent with fluorescence images at the air-water interface before transfer (von Nahmen et al., 1997; Takamoto, 1999). The solid phase is made up primarily of DPPC and PA (Lipp, 1997), and the fluid phase is primarily POPG and protein (Lipp et al., 1998; von Nahmen et al., 1997). The height trace shows that the fluid phase is 1–2 nm lower than the solid phase. This difference is due to the combination of the greater thickness of the solid phase monolayer relative to the fluid phase monolayer, and the greater compressibility of the fluid phase (Marsh, 1990).

Fig. 2 *B* shows an AFM image of the same film transferred at a surface pressure of 55 mN/m and 30°C, above the break in the isotherm. The fluid phase domains (*light gray*) are 4 nm higher than the solid phase (*dark gray*). This shows that the fluid phase has increased in thickness by 5–6 nm in comparison to Fig. 2 *A*, which is roughly equal to a bilayer of POPG (Marsh, 1990). The addition of SP-C*ff* to the lipid mixture induced a two- to three-dimensional phase transition. Instead of being squeezed-out, the unsaturated lipid remains at the interface, although in a multilayer, rather than a monolayer, form. Without the protein, the fluid phase is almost completely removed from the interface (Takamoto, 1999).

DPPC/POPC (palmitoyloleoylphosphatidylcholine), DPPC/PA/POPC, DPPG (dipalmitoylphosphatidylglycerol)/POPG (Takamoto, 1999), and DPPC/DPPG (von Nahmen et al., 1997) lipid mixtures showed similar transitions in the presence of native human recombinant SP-C (von Nahmen et al., 1997) or SP-C*ff* (Takamoto, 1999). SP-C and SP-C*ff* contain a hydrophobic α-helix segment that is capable of spanning a lipid bilayer (Johansson, 1998). At ~50 mN/m surface pressure, the orientation of SP-C likely switches from parallel to perpendicular to the interface, allowing SP-C to bridge the thickened fluid lipids (Gericke et al., 1997; von Nahmen et al., 1997). The thicker fluid phase allows the surface pressure to be distributed over a wider cross section; hence, the absolute force on the fluid domain is smaller than that required to squeeze the lipids out of the interface. On expansion, these thickened patches quickly reincorporate into the monolayer at surface pressures below ~45 mN/m.

Surprisingly, the fluid phase transition depends on the properties of the solid phase. Fig. 1 *C* shows the isotherm of a 3:1 DPPC/POPC lipid mixture with 2 wt % SP-C*ff* at 30°C. Instead of the small break in the isotherm at ~50 mN/m (Fig. 1 *B*), there is a distinct plateau at a pressure of 40 mN/m, and another break in the isotherm at ~55 mN/m on the second compression. Fig. 2 *C* shows an AFM image above the first plateau in the isotherm at 50 mN/m. With no PA in the solid phase, the fluid phase forms multilayer steps rather than uniformly thickening (Fig. 2 *B*). This is the same behavior as observed earlier for 3:1 DPPC/DPPG mixtures with human recombinant SP-C (von Nahmen et al., 1997); hence it appears that the palmitoylated cysteines are not essential for this transition (see sequence information in Materials and Methods). When PA is added to DPPC monolayers, the molecular tilt decreases, increasing the thickness of the monolayer; the molecular ordering becomes longer-ranged, and the temperature range of the solid phase increases (Lipp, 1997; Lee, Majewski, von Nahmen, Gopal, Howes, Kjaer, Smith and Zasadzinski, submitted for publi-

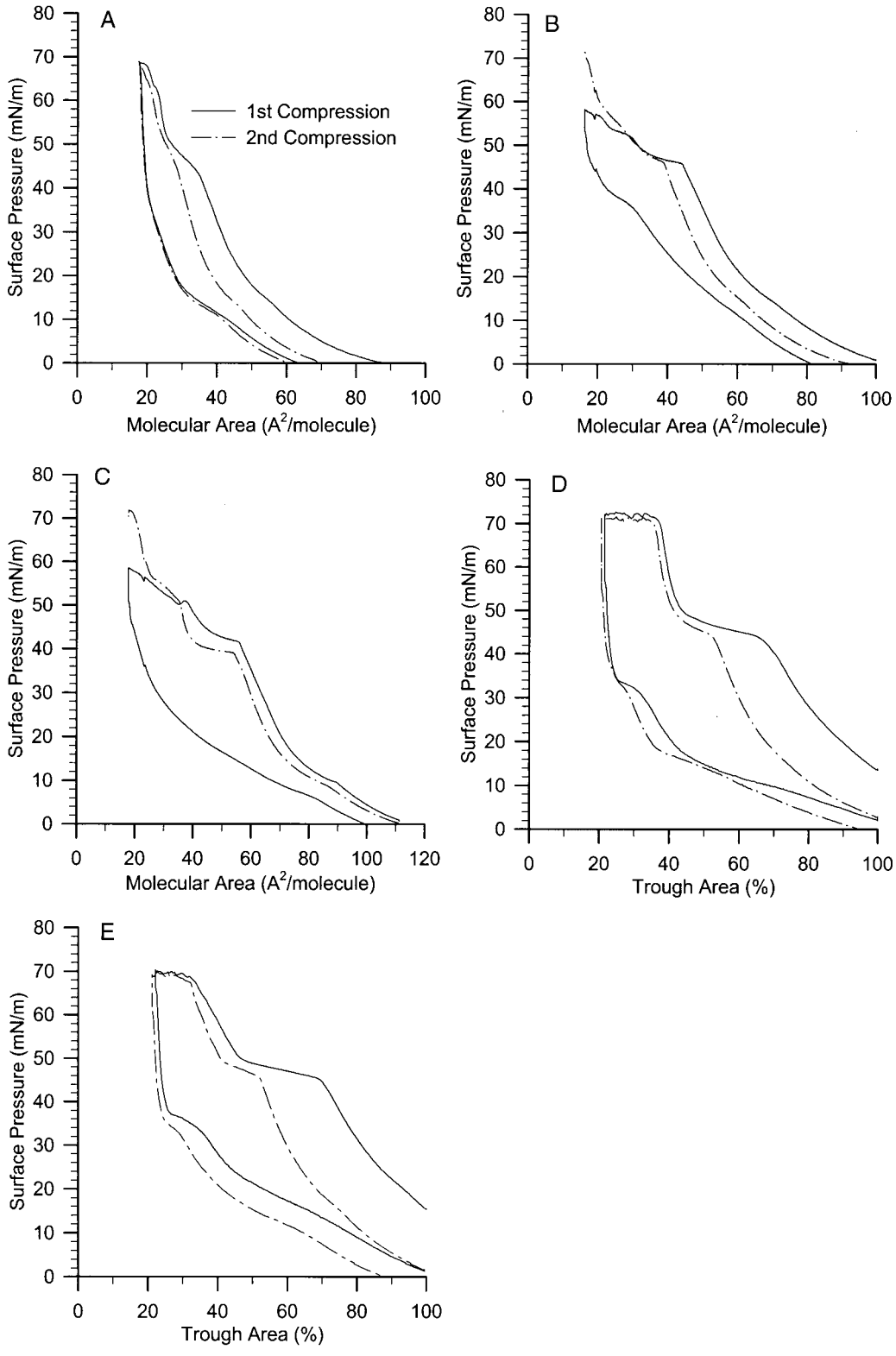

FIGURE 1 (*A*) Quasi-static cycling isotherms (compression–expansion–compression) for a DPPC/POPG/PA, 68:22:8 (wt/wt/wt) lipid mixture on a buffered saline subphase (150 mM NaCl, 5 mM CaCl, 0.2 mM NaHCO3, pH = 6.9) at 30°C. There were no significant variations in any of the isotherms over the temperature range of 30–37°C. Without protein, the second compression shows a significant offset in area per molecule likely due to loss of the unsaturated POPG to the subphase. Subsequent compressions show that the POPG is irreversibly lost and the maximum surface pressure steadily decreases. Surface pressure (reduction in surface tension from the clean interface) is plotted versus the area per lipid molecule in *A–C*. (*B*) Cycling isotherms of the same lipid mixture and subphase as (*A*), but with 2 wt % SP-C*ff* added at 30°C. The plateau in the isotherm at a surface pressure of ~50 mN/m is obvious

cation). These changes likely lead to changes in the mechanical properties of the monolayer. This may explain the benefits obtained by supplementing bovine lung surfactant extract with palmitic acid in the clinically used Survanta. However, the PA fraction in native surfactants extracted by lavage is typically lower and ranges from 0 to 3 wt % (Batenburg and Haagsman, 1998), so the role of PA in natural surfactants is less clear.

To measure monolayer mechanical properties, we have designed and built a magnetic needle monolayer viscometer (Brooks et al., 1999). The basic principle is that a small magnet supported in a Teflon "boat" floating on the monolayer surface is subjected to a constant force using a controlled magnetic field gradient in the plane of the monolayer and oriented along the axis of the "boat." Higher needle velocities correspond to low monolayer viscosity and low needle velocities with high viscosity for a given magnetic force. The velocity is normalized to the speed of the needle on a clean subphase. Fig. 3 shows the normalized needle velocity for a given applied magnetic force for a monolayer of 77 wt % DPPC and 23 wt % POPG with varied PA fractions on a pure water subphase at 25°C. With no PA in the monolayer, the needle velocity is constant for all surface pressures and is nearly the same as for a clean interface with no surfactant (normalized speed of 1). For 10 wt % PA, we see a dramatic decrease in needle velocity at surface pressures from 35 to 40 mN/m, which corresponds to a large increase in viscosity. This PA-induced change in the monolayer rigidity at high surface pressure correlates with the changes in monolayer morphologies between Fig. 2, *B* and *C*. The optimal PA content suggested by Tanaka (Tanaka et al., 1986) in developing Survanta is ~10% by weight. At this PA fraction, there is a high viscosity at high surface pressure, but low viscosity at low surface pressure. This PA fraction also corresponds to changes in the tendency of the monolayer to fold rather than fracture at collapse (Takamoto, 1999). A high viscosity at high surface pressure appears to be necessary for the morphological transitions shown in Fig. 2, but a low viscosity at low surface pressures may be necessary for good monolayer respreading. At 20 wt % PA, the needle velocity begins to decrease on initial compression; by a surface pressure of ~20 mN/m, the film is so rigid that the needle cannot move with the maximum force we can apply.

The net result of adding ~10 wt % PA to the monolayer is that the surface pressure is higher for a given compression with PA than without PA (See Fig. 1, *B* and *C*; compare small break in the isotherm in 1 *B* with the distinct plateau in 1 *C*), and the uniformly thickened fluid phase (Fig. 2 *B*) likely reincorporates more efficiently into the monolayer on expansion than does the step-wise thickened fluid phase without PA (Fig. 2 *C*). This explains one of the benefits derived from supplementing bovine lung surfactant extract with PA in the production of Survanta. Hexadecanol can be substituted for PA and produces similar effects on DPPC packing in the solid phase, and on isotherms and monolayer morphology (Takamoto, 1999). This helps explains the role of hexadecanol in Exosurf, another clinically used replacement surfactant (Poulain and Clements, 1995).

The consistent behavior of SP-C with the wide variety of solid and fluid phase lipids suggests that a similar transition should occur in the more chemically complex bovine lung surfactant extract, Survanta. Fig. 1 *D* shows cyclic isotherms for Survanta at 37°C, which was deposited from the aqueous suspension directly onto the subphase. The isotherm was similar to the model lipid/SPC*ff* mixture shown in Fig. 1 *B*. On the second and subsequent compressions, a small break in the isotherm was present at 45–50 mN/m, just as in the model mixture (Fig. 1 *B*). AFM images of films transferred (Lee et al., 1998) at 45 mN/m (Fig. 2 *D*) and at 55 mN/m (Fig. 2 *E*) at 30°C showed the same transitions as the model mixture. In Fig. 2 *D*, below the break in the isotherm, the solid phase domains (*light gray*) are 1–2 nm thicker than the fluid domains (*dark gray*), similar to Fig. 2 *A*. The small white spots are lipid aggregates trapped during the transfer from the air-water interface to the substrate. Fig. 2 *E* shows the film transferred at 55 mN/m, above the break in the isotherm. As in Fig. 2 *B*, the fluid phase domains are uniformly thicker by 1–2 nm than the solid phase, indicating that the native SP-C in Survanta induces a similar morphological change as SP-C*ff* or the human recombinant SP-C (von Nahmen et al., 1997). The change in thickness is not as great as in the model mixtures, and is not consistent with the thickness of the typical bilayer thickness of ~5 nm. This may be due to the smaller SP-C fraction in Survanta than in the model mixtures or in native surfactant (Walther et al., 1998; Mizuno et al., 1995), the lack of palmitoylation in the SP-C*ff* used in the model mixtures, or to difficulties in

on the first compression. The second and subsequent compressions show a small break in the isotherm at the same surface pressure as the original plateau and the collapse pressure increases to >70 mN/m. The offset in area per molecule is diminished, suggesting that less POPG is lost to the subphase. (*C*) Cycling isotherms of 3:1 DPPC/POPC with 2 wt % SP-C*ff* at 30°C. Instead of the small break in the isotherm at ~50 mN/m (*B*), there is a distinct plateau at a pressure of 40 mN/m, and another break in the isotherm at ~55 mN/m on the second and subsequent compressions. Without PA, the surface pressure for a given compression is less than with PA (*B*). There is even less offset in area per lipid molecule between the first and second cycles in the presence of PA (*B*). (*D*) Cycling isotherms of Survanta on the same subphase as (*A*, *B*) at 30°C. The first compression shows a very similar break in the isotherm as in (*B*), which is retained on subsequent compressions. There appears to be almost no offset in area per molecule after the first compression. (*E*) Cycling isotherms of Survanta with 5 wt % added SP-B_{1-25} peptide at collapse at 37°C. The isotherm is quite similar to that in *D*. The peptide partitions mainly into the fluid phase domains and does not affect the solid phase domains to any great extent.

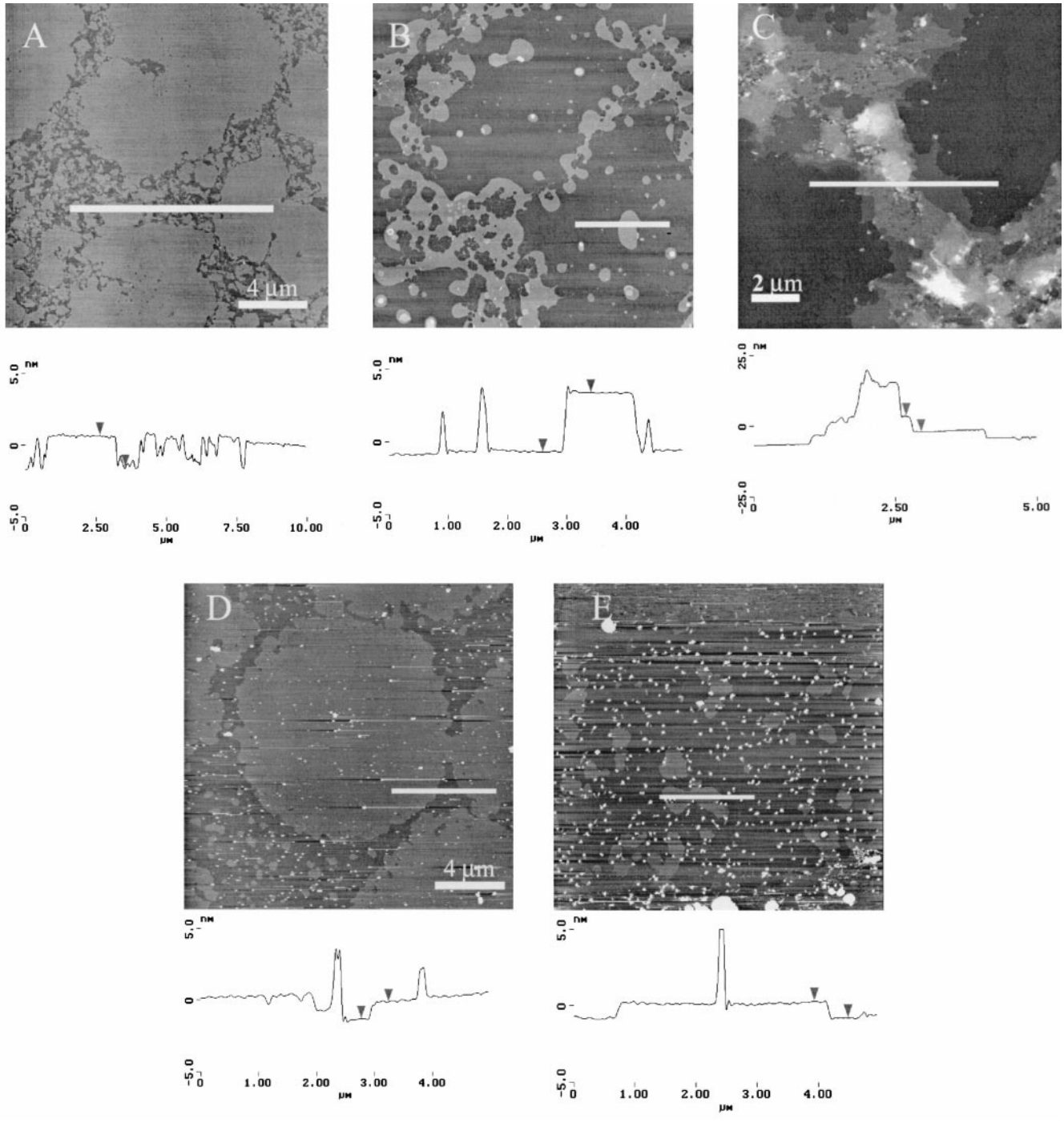

FIGURE 2 (*A*) Contact mode AFM image of model lung surfactant monolayer (DPPC/POPG/PA/SP-C*ff* in weight ratio of 68:22:8:2) transferred from the air-water interface at a surface pressure just below the break in the isotherm (45 mN/m, see Fig. 1 *B*) onto a mica substrate (Lee et al., 1998) at 30°C. The height trace (*white line in image*) shows the solid phase domains (*light gray*) are 1–2 nm thicker than the fluid phase domains (*dark gray*). The solid phase domains consist of all *trans*, extended chains (Lee et al., submitted for publication) and are expected to be thicker and less compressible than the fluid phase domains, which consist of disordered chains (Marsh, 1990). The irregular shape and 5–10 micron size of the solid phase domains are the same as observed at the air-water interface with fluorescence microscopy. (*B*) Contact mode AFM image of the same film (DPPC/POPG/PA/SP-C*ff* in weight ratio of 68:22:8:2) transferred at a surface pressure of 55 mN/m at 30°C, which is above the break in the isotherm. Now, the fluid phase domains are light gray, indicating that the fluid phase is thicker than the solid phase (*dark gray*). The height trace (*white line in image*) shows that the fluid phase is ~4 nm higher than the solid phase. This shows that the fluid phase has increased in thickness by 5–6 nm in comparison to Fig. 2 *A*. (*C*) AFM image of 3:1 DPPC/POPC, with 2 wt % SP-C*ff* transferred at a surface pressure above the first plateau in the isotherm at 50 mN/m and 30°C. When the solid phase consists of only DPPC, the fluid phase forms multilayer steps rather than a uniformly thickened fluid phase (*B*). This stepped morphology is similar to that observed in DPPC/DPPG films with palmitoylated human recombinant SP-C (von Nahmen et al., 1997). (*D*) AFM image of Survanta monolayer transferred at a surface pressure of 45 mN/m at 30°C, just below the plateau in the isotherm. The fluid phase (*dark gray*) is 1–2 nm lower than the solid phase domains

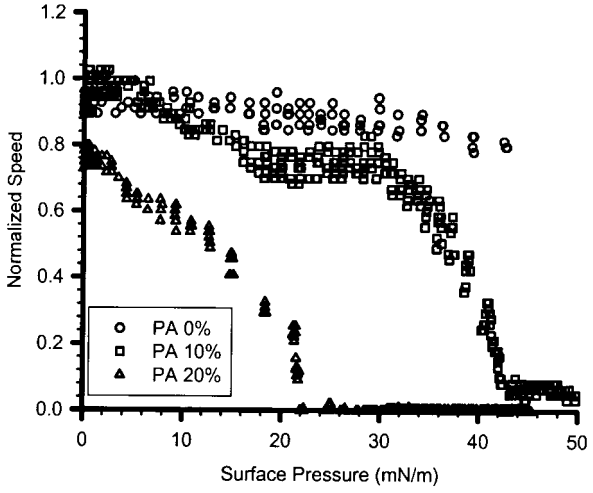

FIGURE 3 The speed of a magnetic needle floating on a surfactant-covered interface at a given magnetic force was measured as a function of surface pressure for DPPC/POPG (77:23, wt/wt) monolayers with differing PA content on a pure water subphase at 25°C. The speed is normalized to the needle velocity on a clean, surfactant-free interface. A high needle velocity corresponds to a low monolayer viscosity, although it is difficult to assign a single value to the viscosity of a non-Newtonian monolayer. With no PA in the monolayer, the needle velocity is nearly independent of surface pressure and is not significantly different from a clean interface (normalized speed of 1). For a PA fraction of 10%, there is a transition between 30 and 40 mN/m from high needle velocity to low needle velocity. This change in the monolayer mechanical properties correlates with a change in the morphological transitions in Fig. 2 and with the collapse structures seen in Fig. 4. For 20 wt % PA, the monolayer is much stiffer, and by 20 mN/m, we cannot drive the needle across the interface with the maximum force we can apply. For surface pressures >50 mN/m, the needle often sinks and we cannot measure surface viscosity.

transfer for AFM of the more complex mixtures. Higher SP-C*ff* fractions likely led to a proportionately greater change in the fluid phase thickness in the model mixtures (Takamoto, 1999). The uniform change in thickness of the fluid phase domains is likely due to the PA added to Survanta. SP-B can also lead to the formation of a monolayer to multilayer transition in the fluid phase lipids (Krol et al., 2000; Lipp et al., 1998). Mixture of native SP-B and SP-C with phosphatidylcholines show a similar thickening transition by AFM (Grunder et al., 1999), although the morphology of the multilayer patches is less well defined and smaller with SP-B than with SP-C (Krol et al., 2000; Lipp et al., 1998).

While SP-C is responsible for helping maintain the fluid lipids in the vicinity of the air-water interface, the SP-B protein modifies monolayer collapse, thereby ensuring reproducibly low surface tensions (Lipp et al., 1998). Fig. 4 *A* shows a fluorescence microscopy image of a 67:22:8:3 (wt/wt/wt/wt) DPPC/POPG/PA/full length SP-B_{1-78} with 0.5 mol % of the fluorescent probe NBD-PG at the collapse pressure of 65 mN/m at 37°C. The monolayer undergoes a three-dimensional buckling into the subphase (*bright area in center of image*), but maintains the monolayer morphology of solid phase domains (*dark*) in a continuous fluid phase (*bright*) not only at the interface, but throughout the folded region. There is no loss of material to the subphase on collapse. The buckled areas reincorporate into the monolayer on expansion over a range of surface pressures from the collapse pressure to ~10 mN/m.

Fig. 4 *B* shows a fluorescence image of Survanta at its collapse pressure at 37°C. The bright streak is a fracture in the monolayer. These fractures are similar to those in pure DPPC monolayers (Lipp, 1997) at collapse, and lead to inefficient respreading. The monolayer exhibits the similar bright-dark, solid-fluid coexistence as the model mixture, although the domain sizes are smaller. It is estimated that the amount of SP-B in Survanta is only ~0.1 wt % (Walther et al., 1997; Taeusch et al., 1986), while the amount of SP-B in native surfactant is closer to 1.5–2 wt % (Mizuno et al., 1995). However, the exact amount of SP-B, SP-C, or lipid in any native surfactant or surfactant extract has not been accurately measured because reliable methods of harvesting surfactant from the alveoli are not available (Mizuno et al., 1995). When 5 wt % SP-B_{1-25} is added to the Survanta suspension, collapse occurs via buckling (Fig. 4 *C*), just as in the model mixture with protein (Fig. 4 *A*). The folded regions of the monolayer have similar morphology, and likely composition, to the rest of the monolayer. The folded material rapidly reincorporates into the monolayer on expansion, again over a range of surface pressure from collapse to ~15 mN/m. Fig. 1 *E* shows the cycling isotherms of Survanta with 5 wt % added SP-B_{1-25} peptide at collapse at 37°C. The isotherm is quite similar to that in Fig. 1 *D*. The peptide partitions mainly into the fluid phase domains and does not affect the solid phase domains to any great extent. From these and earlier results (Lipp et al., 1998), the folding transition is relatively independent of the details of the lipid composition of the monolayer. There is also a minimum fraction of SP-B required in the monolayer to induce the monolayer folding transition. A minimum fraction of SP-B is also necessary for optimal surfactant performance in vivo. Adding native SP-B (Mizuno et al., 1995)

as shown on the height trace. The bright white specks across the image are small aggregates of Survanta dispersed in the aqueous phase that were trapped during transfer. (*E*) AFM image of Survanta monolayer transferred at a surface pressure of 55 mN/m and 30°C, just above the plateau in the isotherm. The solid phase is now dark gray and the fluid phase is lighter gray. As in *B*, the fluid phase domains have thickened, but here they are only 1–2 nm higher than the solid phase domains. As the amount of thickening of the fluid domains scales with the amount of SP-C present, this may be consistent with a smaller fraction of SP-C in Survanta than in the model films. Overall, the general features of Survanta films appear very similar to the DPPC/POPG/PA/SP-C*ff* films shown in *B*.

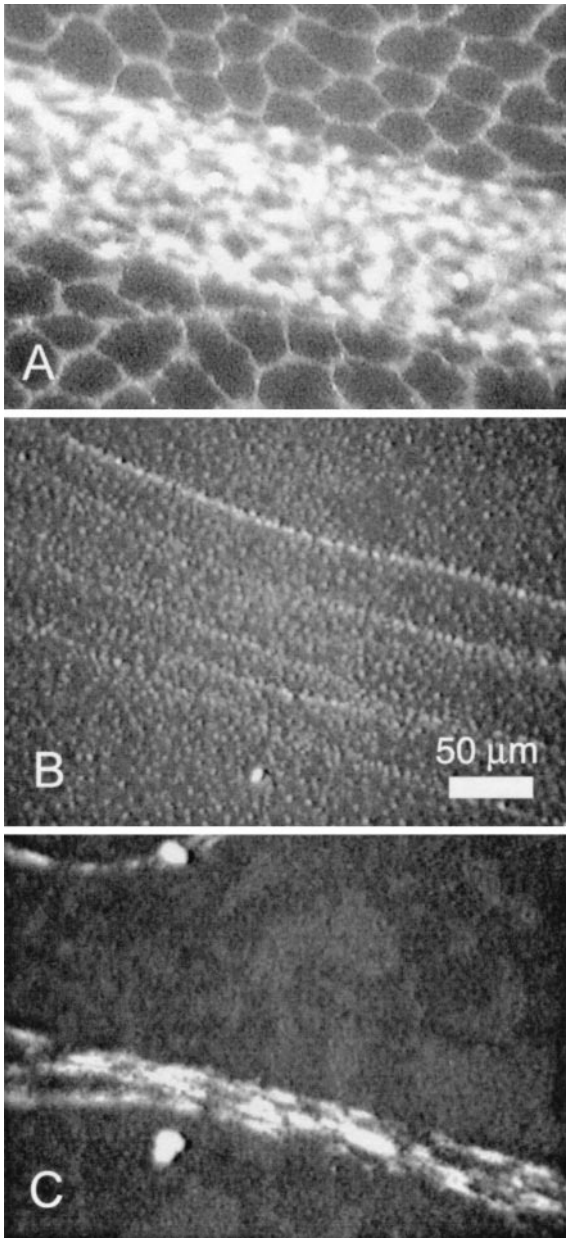

FIGURE 4 (*A*) Fluorescence optical micrograph of coexisting monolayer and folded region in a film of DPPC/POPG/PA/SP-B_{1-78}, in weight ratio 68:22:8:3 at the collapse pressure of 65 mN/m at 37°C. The bright fluid phase network (likely containing POPG, the protein and the fluorescent lipid, which separates into disordered phases) separates the darker solid phase domains (probably containing the DPPC and PA) both in the monolayer and in the folded region (Lipp et al., 1998). The organization and distribution of the domains remains the same within the folds, implying that the composition also remains the same. The folds reincorporate into the monolayer on expansion over a range in surface pressure from the collapse pressure to ~15 mN/m. The folds always protrude into the subphase. Without SP-B the films do not fold, but rather fracture, as in Fig. 4B. (*B*) Fluorescence image of Survanta at 37°C at collapse showing a similar solid-fluid phase coexistence (see Fig. 4A), although with significantly smaller domains. At collapse, Survanta fractures to form bright cracks at the interface. The materials in and around the cracks are slow to respread on expansion of the monolayer. (*C*) Fluorescence image of Survanta with 5 wt % added SP-B_{1-25} peptide at collapse at 37°C. As in Fig. 4B, there is solid-fluid phase coexistence with a small domain size, but the added SP-B causes the monolayer to undergo a reversible folding as in the model mixture (Fig. 4A). The folds are somewhat smaller than in the model mixture and appear to scale with the domain size. The folded regions appear to have the same overall composition as the rest of the monolayer, and reincorporate readily into the monolayer on expansion.

or SP-B_{1-25} peptide (Walther et al., 1997) to Survanta improves oxygenation and other measures of surfactant performance in animals. Antibodies to SP-B or a genetic deficiency of SP-B causes respiratory failure (Robertson and Halliday, 1998; Tokieda et al., 1997).

Correlating morphological and isotherm measurements of Langmuir monolayers to the organization and mechanics of the surfactant within the alveoli during normal breathing is much more problematic. The maximum static surface tension within excised rabbit lungs was measured to be ~30 mN/M (surface pressure of ~40 mN/m) (Bachofen et al., 1987), while the minimum surface tension has been estimated to be close to zero (Bachofen et al., 1987; Schürch et al., 1976, 1978). No measurements have been done of the dynamic surface tension during the normal respiratory cycle, so the range of surface tensions during actual breathing is unknown. The maximum surface tension (minimum surface pressure) on a Langmuir trough depends on the mode of deposition of surfactant and the concentration, if any, of surfactant in the subphase, but can range from 40 (Schürch et al., 1976, 1978) to 70 mN/m (surface pressures of 30–0 mN/m). In our experiments, the surface pressure was forced to cycle between zero and the collapse pressure of the particular surfactant mixture by varying the surface area; it is unclear if either the maximum or minimum surface pressure shown in the isotherms are reached during breathing. However, both of the prominent morphological transitions we have observed—the multilayer formation induced by SP-C in the fluid phase domains and the folding transition at collapse induced by SP-B—occur at surface pressures between 40 and 70 mN/m on compression, which shows that these are within the range of measured maximum and minimum surface tensions in static lungs.

The change in surface area of the lungs during breathing is an important corollary to the range of surface tension during breathing. When lung volume changes from 40 to 100% of total lung capacity, the lung epithelial cell basal surface area increases 35% (Tschumperlin and Margulies, 1999). However, the actual area change of the air-fluid interface is more difficult to measure (Wirtz and Dobbs, 2000). Secretion of surfactant from the type II cell is postulated to be induced by deep sighing breaths and the resulting large increases in the lung volume and surface area (Wirtz and Dobbs, 2000). The change in relative area in Langmuir isotherms is arbitrary; the monolayer area is changed sufficiently so that the entire range between the collapse pressure and zero surface pressure is recorded. The relative change in surface pressure for a given change in

area is typically much greater on expansion than on compression of the monolayer (see Fig. 1), especially at high surface pressures after monolayer collapse. Hence, a given change in area could result in a much larger change in surface pressure depending on the history of the monolayer. The folds in the collapsed monolayer (Fig. 4) or the multilayers in the fluid domains (Fig. 2) revert back to the monolayer over a range of surface pressures from the collapse pressure to as low as 15 mN/m. It is unclear if the change in surface area during normal breathing would cause these structures to occur or disappear on each breathing cycle.

CONCLUSIONS

Although the clinical importance of the LS proteins SP-B and SP-C is well established (Tanaka et al., 1986; Poulain and Clements, 1995; Hawgood et al., 1998; Goerke, 1998; Johansson, 1998), the role of these proteins in altering the properties of surfactant monolayers remains ambiguous. It is also relatively well established that the fatty acid and unsaturated lipid components of lung surfactant are important to the proper function of surfactant at all stages of the compression and expansion cycle (Veldhuizen et al., 1998), although the exact fraction of any lipid in lung surfactants is still not well established. Direct imaging with fluorescence and atomic force microscopy clearly show that the interactions between SP-B, SP-C, and palmitic acid with the remaining lipid components of synthetic and animal extract surfactants are non-ideal and lead to novel morphologies likely to be important to LS function. Establishing the properties of SP-B, SP-C, and PA are essential to determining the composition of an effective synthetic surfactant and in evaluating synthetic peptide function.

SP-C retains a continuous fluid phase network of unsaturated lipids and proteins, separating islands of solid phase lipids up to monolayer collapse. The nature of the fluid phase transition depends on the lipid composition: when PA is present in the monolayer, the fluid phase thickens uniformly, while without PA, the fluid phase forms multilayer stacks. Native SP-C, palmitoylated, human recombinant SP-C (von Nahmen et al., 1997), and SP-C*ff* appear to have very similar effects on the monolayer.

With SP-B, collapse occurs by a reversible buckling in which the monolayer is flexible enough to fold, while retaining sufficient cohesion to prevent loss of material to the subphase. The folds have the same composition as the monolayer, and reversibly reincorporate into the monolayer on expansion. Both the full length protein, SP-B_{1-78}, and the SP-B_{1-25} peptide are capable of inducing this folding transition.

PA, when added to DPPC monolayers, increases the monolayer viscosity at high surface pressures, but not at low surface pressure. This increased monolayer rigidity at high surface pressures appears to be necessary to allow homogeneous multilayer formation in the fluid phase via SP-C and the folding collapse mechanism in films also containing SP-B. Higher fractions of PA likely make the monolayer too rigid to respread.

These two- to three-dimensional transitions allow collapse to occur at elevated surface pressures while making it possible for the protein and unsaturated lipid components to remain associated with the monolayer, facilitating rapid respreading. Without the proteins, the fluid phase lipids are squeezed-out from the monolayer, leaving behind a rigid DPPC-rich monolayer that fractures irreversibly at collapse. These morphological transitions of multilayer formation, followed by a folding and unzipping process, explains how lung surfactant can both achieve low surface tensions and respread readily from the collapsed state, without the need to undergo any compositional refinement upon compression. The presence of the protein-containing folds extending into the subphase at high compression may also provide a mechanism for incorporation of new material to the interface upon expansion. A thorough understanding of the roles of the lipids and proteins in lung surfactant can provide a mechanism-based rationale for the design of replacement surfactants for treatment of respiratory distress syndrome.

J.D., K.Y.C.L., M.M.L., and J.A.Z. were supported by National Institutes of Health Grant HL-51177; J.A.Z. and A.J.W. were also supported by the Tobacco Related Disease Research Program Grant 8RT-0077. J.D. was supported by Tobacco Related Disease Research Program Grant 8DT-0171. A.J.W. was also supported by National Institutes of Health Grant HL55534, the Drew RCMI Bioinformatics Core (NCRR/RCMI G12 RR 03026), and National Institutes of Health Small Equipment Grant GM 50483. K.Y.C.L. was supported by the March of Dimes Award (5-FY98-0728), the Searle Scholars Program/The Chicago Community Trust (99-C-105), the American Lung Association (RG-085-N), and the Packard Foundation (99-1465).

REFERENCES

Bachofen, H., S. Schürch, M. Urbinelli, and E. R. Weibel. 1987. Relations among alveolar surface tension, surface area, volume and recoil pressure. *J. Appl. Physiol.* 62:1878–1887.

Bastacky, J., C. Y. Lee, J. Goerke, H. Koushafar, D. Yager, T. P. Speed, Y. Chen, and J. A. Clements. 1995. Alveolar lining layer is thin and continuous: low temperature scanning electron microscopy of rat lung. *J. Appl. Physiol.* 79:1615–1628.

Batenburg, J. J., and H. P. Haagsman. 1998. The lipids of pulmonary surfactant: dynamics and interactions with proteins. *Progress in Lipid Research.* 37:235–276.

Bernhard, W., J. Mottaghian, A. Gebert, G. A. Rau, H. von der Hardt, and C. F. Poets. 2000. Commercial versus native surfactants. *Am. J. Crit. Care Med.* 162:1524–1533.

Brooks, C. F., G. G. Fuller, C. W. Frank, and C. R. Robertson. 1999. An interfacial stress rheometer to study rheological transitions in monolayers at the air-water interface. *Langmuir.* 15:4367–4373.

Bruni, R., H. Taeusch, and A. Waring. 1991. SP-B: Lipid interactions of synthetic peptides representing the amino-terminal amphipathic domain. *Proc. Natl. Acad. Sci. USA.* 88:7451–7455.

Cochrane, C., and S. Revak. 1991. SP-B: Structure-function relationships. *Science.* 254:566–568.

Davis, A. J., A. H. Jobe, D. Hafner, and M. Ikegami. 1998. Lung function in premature lambs and rabbits treated with a recombinant SP-C surfactant. *Am. J. Respir. Crit. Care Med.* 157:553–559.

Gericke, A., C. R. Flach, and R. Mendelsohn. 1997. Structure and orientation of lung surfactant SP-C and L-a DPPC in aqueous monolayers. *Biophys. J.* 73:492–499.

Goerke, J. 1998. Pulmonary surfactant: functions and molecular composition. *Biochim. Biophys. Acta.* 1408:79–89.

Gordon, L. M., S. Horvath, M. Longo, J. A. Zasadzinski, H. W. Taeusch, K. Faull, C. Leung, and A. J. Waring. 1996. Conformation and molecular topography of the N-terminal segment of surfactant protein B in structure-promoting environments. *Protein Sci.* 5:1662–1675.

Gordon, L. M., K. Y. C. Lee, M. M. Lipp, J. A. Zasadzinski, F. J. Walther, M. A. Sherman, and A. J. Waring. 2000. Lipid conformation of the N-terminal segment of surfactant protein B determined with C13-enhanced Fourier transform infrared spectroscopy. *J. Peptide Res.* 55: 330–347.

Grunder, R., P. Gehr, H. Bachofen, S. Schürch, and H. Siegenthaler. 1999. Structures of surfactant films: a scanning force microscopy study. *Eur. Respir. J.* 14:1290–1296.

Hawgood, S., M. Derrick, and F. Poulain. 1998. Structure and properties of surfactant protein B. *Biochim. Biophys. Acta.* 1408:150–160.

Ikegami, M., A. D. Horowitz, J. A. Whitsett, and A. H. Jobe. 1998. Clearance of SP-C and recombinant SP-C in vivo and in vitro. *Am. J. Physiol. Lung Cell Mol. Physiol.* 274:L933–L939.

Ikegami, M., and A. H. Jobe. 1998. Surfactant protein-C in ventilated premature lamb lung. *Pediat. Res.* 44:860–864.

Ingenito, E. P., L. Mark, J. Morris, F. F. Espinosa, R. D. Kamm, and M. Johnson. 1999. Biophysical characterization and modeling of lung surfactant components. *J. Appl. Physiol.* 86:1702–1714.

Jobe, A. H. 1998. Hot topics in and new strategies for surfactant research. *Biology of the Neonate.* 74:3–8.

Johansson, J. 1998. Structure and properties of surfactant protein C. *Biochim. Biophys. Acta.* 1408:161–172.

Knobler, C. M., and R. C. Desai. 1992. Phase transitions in monolayers. *Annu. Rev. Phys. Chem.* 43:207–236.

Krol, S., M. Ross, M. Sieber, S. Kunneke, H.-J. Galla, and A. Janshoff. 2000. Formation of three-dimensional protein-lipid aggregates in monolayer films induced by surfactant protein B. *Biophys. J.* 79:904–918.

Krueger, M. A., and D. P. I. Gaver. 2000. A theoretical model of pulmonary surfactant monolayer collapse under oscillating area conditions. *J. Colloid Interface Sci.* 299:353–364.

Lee, K. Y. C., M. M. Lipp, D. Y. Takamoto, E. Ter-Ovanesyan, and J. A. Zasadzinski. 1998. From free-standing to transferred films: an apparatus for the continuous monitoring of surface morphology via fluorescence and atomic force microscopy. *Langmuir.* 14:2567–2572.

Lipp, M. M. 1997. A Microscopy Study of Model Lung Surfactant Monolayers. Ph.D. Thesis, University of California, Santa Barbara.

Lipp, M. M., K. Y. C. Lee, D. Y. Takamoto, J. A. Zasadzinski, and A. J. Waring. 1998. Coexistence of buckled and flat monolayers. *Phys. Rev. Lett.* 81:1650–1653.

Lipp, M. M., K. Y. C. Lee, A. J. Waring, and J. A. Zasadzinski. 1997a. Design and performance of an integrated fluorescence, polarize fluorescence, and Brewster angle microscope/Langmuir trough system for the study of lung surfactant monolayers. *Review of Scientific Instruments.* 68:2574–2582.

Lipp, M. M., K. Y. C. Lee, J. A. Zasadzinski, and A. J. Waring. 1996. Phase and morphology changes induced by SP-B protein and its amino-terminal peptide in lipid monolayers. *Science.* 273:1196–1199.

Lipp, M. M., K. Y. C. Lee, J. A. Zasadzinski, and A. J. Waring. 1997b. Fluorescence, polarized fluorescence and Brewster angle microscopy of palmitic acid and lung surfactant protein B monolayers. *Biophys. J.* 72:2783–2804.

Longo, M., A. Bisagno, J. Zasadzinski, R. Bruni, and A. Waring. 1993. A function of lung surfactant protein SP-B. *Science.* 261:453–456.

Marsh, D. 1990. CRC Handbook of Lipid Bilayers. CRC Press, Inc., Boca Raton, FL.

Mizuno, K., M. Ikegami, C. M. Chen, T. Ueda, and A. H. Jobe. 1995. Surfactant protein B supplementation improves in vivo function of a modified natural surfactant. *Pediat. Res.* 37:271–276.

Nag, K., J. Perez-Gil, M. L. F. Ruano, L. A. D. Worthman, J. Stewart, C. Casals, and K. M. W. Keough. 1998. Phase transitions in films of lung surfactant at the air-water interface. *Biophys. J.* 74:2983–2995.

Poulain, F. R., and J. A. Clements. 1995. Pulmonary surfactant therapy. *West. J. Med.* 162:43–50.

Robertson, B., and H. L. Halliday. 1998. Principles of surfactant replacement. *Biochim. Biophys. Acta.* 1408:346–361.

Schürch, S., J. Goerke, and J. A. Clements. 1976. Direct determination of surface tension in the lung. *Proc. Natl. Acad. Sci. USA.* 73:4698–4702.

Schürch, S., J. Goerke, and J. A. Clements. 1978. Direct determination of volume and time-dependence of alveolar surface tension in excised lungs. *Proc. Natl. Acad. Sci. USA.* 75:3417–3421.

Schürch, S., F. H. Y. Green, and H. Bachofen. 1998. Formation and structure of surface films: captive bubble surfactometry. *Biochim. Biophys. Acta.* 1408:180–202.

Taeusch, H. W., K. M. W. Keough, M. Williams, R. Slavin, E. Steele, A. S. Lee, D. Phelps, N. Kariel, J. Floros, and M. E. Avery. 1986. Characterization of bovine surfactant for infants with respiratory distress syndrome. *Pediatrics.* 77:572–581.

Takamoto, D. Y. 1999. Structure and Function of Novel Engineered Thin Films. Ph.D. Thesis, University of California, Santa Barbara.

Tanaka, Y., T. Tsunetomo, A. Toshimitsu, K. Masuda, K. Akira, and T. Fujiwara. 1986. Development of synthetic lung surfactants. *J. Lipid Res.* 27:475–485.

Tchoreloff, P., A. Gulik, B. Denizot, J. E. Proust, and F. Puisieux. 1991. A structural study of interfacial phospholipid and lung surfactant layers by TEM after Blodgett sampling: influence of surface pressure and temperature. *Chem. Phys. Lipids.* 59:151–165.

Tokieda, K., J. A. Whitsett, J. C. Clark, T. E. Weaver, K. Ikeda, K. B. McConnell, A. H. Jobe, M. Ikegami, and H. S. Iwamoto. 1997. Pulmonary dysfunction in neonatal SP-B deficient mice. *Am. J. Physiol. Lung Cell Mol. Physiol.* 273:L875–L882.

Tschumperlin, D. J., and S. S. Margulies. 1999. Alveolar epithelial surface area-volume relationship in isolated rat lungs. *J. Appl. Physiol.* 86: 2026–2033.

Veldhuizen, R., K. Nag, S. Orgeig, and F. Possmayer. 1998. The role of lipids in pulmonary surfactant. *Biochim. Biophys. Acta.* 1408:90–108.

von Nahmen, A., M. Schenk, M. Sieber, and M. Amrein. 1997. The structure of a model pulmonary surfactant as revealed by scanning force microscopy. *Biophys. J.* 72:463–469.

Walther, F. J., J. Hernandez-Juviel, R. Bruni, and A. J. Waring. 1997. Spiking Survanta with synthetic surfactant peptide improves oxygenation in surfactant-deficient rats. *Amer. J. Respir. Crit. Care Med.* 156:855–861.

Walther, F. J., J. Hernandez-Juviel, R. Bruni, and A. J. Waring. 1998. Protein composition of synthetic surfactant affects gas exchange in surfactant-deficient rats. *Pediatric Res.* 43:666–673.

Wirtz, H. R., and L. G. Dobbs. 2000. The effects of mechanical forces on lung functions. *Resp. Physiol.* 119:1–17.